Original Article

Prostate magnetic resonance imaging (MRI) in patients with hip implants—presetting a protocol using a phantom

Yuriy A. Vasilev[1]^, Olga Yu. Panina[1,2]^, Dmitry S. Semenov[1]^, Ekaterina S. Akhmad[1]^, Kristina A. Sergunova[3]^, Stanislav A. Kivasev[4]^, Alexey V. Petraikin[1]^

[1]State Budget-Funded Health Care Institution of the City of Moscow "Research and Practical Clinical Center for Diagnostics and Telemedicine Technologies of the Moscow Health Care Department", Moscow, the Russian Federation; [2]Moscow State Budgetary Healthcare Institution "Oncological Center No. 1 of Moscow City Hospital named after S.S. Yudin, Moscow Health Care Department", Moscow, the Russian Federation; [3]"CAPSTROYCITY", Moscow, the Russian Federation; [4]Central Clinical Hospital "RZD-Medicine", Moscow, the Russian Federation

Contributions: (I) Conception and design: YA Vasilev, OY Panina; (II) Administrative support: DS Semenov; (III) Provision of study materials or patients: OY Panina, SA Kivasev; (IV) Collection and assembly of data: YA Vasilev, DS Semenov, AV Petraikin; (V) Data analysis and interpretation: OY Panina, ES Akhmad, KA Sergunova; (VI) Manuscript writing: All authors; (VII) Final approval of manuscript: All authors.

Correspondence to: Olga Yu. Panina, MD. State Budget-Funded Health Care Institution of the City of Moscow "Research and Practical Clinical Center for Diagnostics and Telemedicine Technologies of the Moscow Health Care Department", Petrovka Str., 24, 127051, Moscow, the Russian Federation; Moscow State Budgetary Healthcare Institution "Oncological Center No. 1 of Moscow City Hospital named after S.S. Yudin, Moscow Health Care Department", Zagorodnoye str., 18A, 17152, Moscow, the Russian Federation. Email: PaninaOY1@zdrav.mos.ru.

Background: Metal structures are a source of artifacts that significantly complicate the interpretation of magnetic resonance imaging (MRI). The use of prostate MRI as a preliminary test in men with a suspicion on prostate cancer leads to an increased use of the test. The aim of this study was to solve a clinically significant problem: to ensure the reduction of artifacts from metal hip implants during prostate MRI. Another goal was to evaluate the impact of artifact reduction methods on quantitative measurements.

Methods: The prostate gland (PG) phantom model was a cylinder filled with an aqueous solution of polyvinylpyrrolidone at the concentrations of 40%, 30%, and 20% [central zone (CZ), peripheral zone (PZ), and "lesion", respectively]. Phantom MRI study was conducted on Philips Ingenia 1.5T and Philips Ingenia 3T scanners.

Results: For 1.5 T, the reduction in the influence of artifacts inside region of interest (ROI) was observed, expressed in a decrease in the average apparent diffusion coefficient (ADC) (CZ, PZ, "lesion") for the manual artifact reduction (MAR) and ZOOM (title of software artifact reduction) techniques compared to the standard method. For 3T this effect was not detected. The same ADC results were obtained for Standard and MAR techniques, and increased ADC values for ZOOM. Despite the fact that the spread of ADC values on 3.0T scanners was minimal, there was a significant deviation of ADC values from the reference ones (up to 30.4%). Therefore, it is necessary to use a correction coefficient in the ADC calculation for the 3.0 T device. In the presented clinical case, high-quality tomograms were obtained without any artifacts, despite the presence of two hip replacement devices in the scanning area.

Conclusions: The accurate prostate MRI in the presence of implants is essential for an accurate diagnosis. This approach allows to reduce artifacts from hip implants, to visualize PG and periprostatic tissue in the best way, and to detect malignant and benign changes.

^ ORCID: Yuriy A. Vasilev, 0000-0002-5283-5961; Olga Yu. Panina, 0000-0002-8684-775X; Dmitry S. Semenov, 0000-0002-4293-2514; Ekaterina S. Akhmad, 0000-0002-8235-9361; Alexey V. Petraikin, 0000-0003-1694-4682; Kristina A. Sergunova, 0000-0002-9596-7278; Stanislav A. Kivasev, 0000-0003-1160-5905.

Keywords: Magnetic resonance imaging (MRI); prostate cancer; quality assessment; metal artifact; phantom modeling

Submitted Mar 26, 2024. Accepted for publication Sep 09, 2024. Published online Sep 26, 2024.
doi: 10.21037/qims-24-604
View this article at: https://dx.doi.org/10.21037/qims-24-604

Introduction

Magnetic resonance imaging (MRI) is the leading method of assessing prostate cancer using the scale PI-RADS (Prostate Imaging and Reporting and Data System) (1-3). The main pulse sequences are diffusion-weighted images (DWI), T2 weighted images (T2-WI) and dynamic contrast enhanced (DCE) MRI. DWI is a key for assessing a peripheral zone, which is the most common localization of clinically significant prostate cancer (2,4). DWI and apparent diffusion coefficient (ADC) maps are the sequences that share higher sensitivity to artifact (5). Prostate DWI is usually obtained using a spin-echo (SE) sequence with echo-planar imaging (EPI). SE EPI is particularly sensitive to inhomogeneities of the B_0 field due to, among other reasons, metal structures (6,7). At the same time, total hip replacement (THR), being one of the most common surgical procedures in the world, is the effective intervention for degenerative joint diseases applied in patients whose average age is 63 years (8). Thus, MRI implementation, as a method of choice for diagnosis of prostate cancer, together with a spread of hip arthroplasty is a potential problem.

To reduce the area of artifacts, various correction methods are used, including manual and ready-to-use software solutions, applicable for the prostate MRI as well (9-12). ADC is a potentially important biomarker. The variability of this quantitative parameter prevents its wider use in routine radiology, namely, radiomics and differentiating prostate cancer from healthy prostate and prostatitis (13-15). In addition to distortion, metal implants can affect the accuracy of ADC measurement. Generation of a new scanning protocol takes a significant amount of time. As a result, a reception and scanning procedure for a particular patient will be significantly longer, and the work schedule of diagnostic room will be disrupted. Also, if the protocol setting for a patient with an implant is carried out directly during the study, it can lead to implant heating (16). Thus, the phantom makes the preliminary setup more comfortable and efficient: There is no risk for the patient and the phantom parameters are known (17).

The main purpose of this study was to provide MR images of improved quality in patients with THR. The task was to develop a phantom for presetting a prostate scanning protocol in patients with metal implants. Another goal was to evaluate the impact of artifact reduction methods (manual and software) on quantitative ADC measurements.

Methods

Phantom

A model of the prostate gland (PG) is a cylinder with dimensions of 45×45×56 mm, printed on a 3D printer by the selective laser sintering method (18). The model has 3 sections inside (*Figure 1A*,*1B*) to simulate the central (CZ), peripheral (PZ) zones, tumor ("lesion"). In order adjust the model to the ADC values in each prostatic region, the former was filled with the aqueous solution of polyvinylpyrrolidone (PVP) at the concentrations of 40%, 30%, and 20% (CZ, PZ, and "lesion", respectively). These indicators of PVP concentration correspond to ADC values =$(1{,}000\pm36)\times10^{-6}$, $(1{,}230\pm39)\times10^{-6}$ and $(1{,}410\pm36)\times10^{-6}$ mm^2/s, respectively (19). The choice of ADC values for the phantom was based on the experiment results (10,19,20). We scanned these solutions in the previous study performed for the quality control in ADC measurements (19).

A titanium alloy implant for the total hip arthroplasty (*Figure 1C*) was placed in the phantom next to the PG model in order to obtain geometric and other distortions in the images. The PG model together with the implant were placed in a plastic container which was about 6 liters in volume. The container was filled with MRI contrast agent and water to simulate a human body.

MRI scanning

The MRI study was conducted on Philips Ingenia 1.5T and Philips Ingenia 3T scanners. Maximum amplitude for each axis was 45 mT/m. To perform the study, a body radiofrequency coil was installed and fixed on top of the

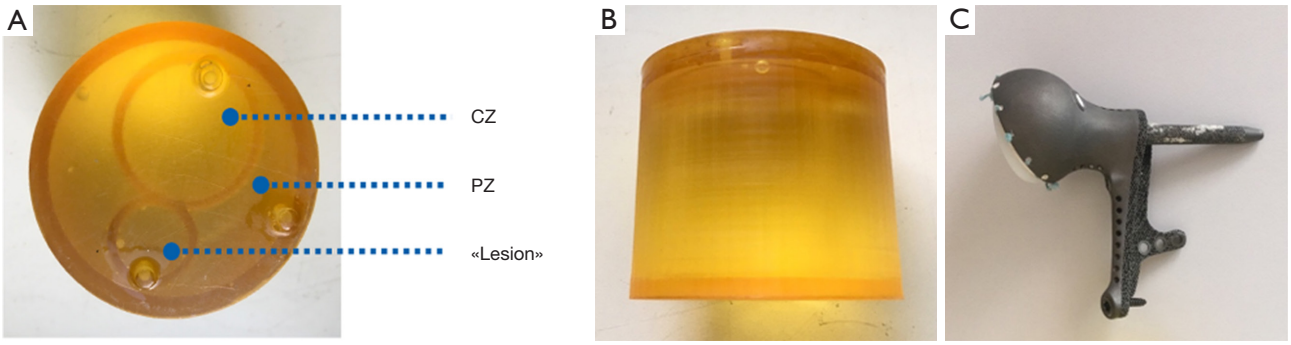

Figure 1 PG model and implant. (A) PG model, top view, (B) PG model, side view, (C) metal implant. CZ, central zone; PZ, peripheral zone; PG, prostate gland of prostate.

plastic container.

A phantom was scanned according to the protocols for T2 TSE and three DWI methods: standard, manual artifact reduction (MAR) and software (ZOOM) corrected ones. A standard protocol was routine for the particular scanner in PG study. A classic single-shot sequence was not also included in the test because it's was not routine for these scanners. Philips Ingenia 1.5T included T2 TSE WI sequence: repetition time (TR)/echo time (TE) 2,776/100 ms, flip angle 90°, field of view (FOV) 70 mm, slice thickness 3 mm, spacing between slices 3 mm, number of averages 3, Bandwidth per pixel 167 Hz, matrix size 176×176. Diffusion-weighted imaging. Standard: TR/TE 3,965.155/86 ms, echo train length 49, flip angle 90°, FOV 300×300 mm, number of averages 2, slice thickness 3 mm, spacing between slices 3 mm, Bandwidth per pixel 1,035 Hz, matrix size 288×288, b-value 0, 1,400 s/mm^2. MAR: TR/TE 3,965.155/175.574 ms, echo train length 99, flip angle 90°, FOV 70×70 mm, number of averages 3, slice thickness 3 mm, spacing between slices 3, Bandwidth per pixel 2,225 Hz, matrix size 80×80, b-value 0, 1,400 s/mm^2. ZOOM: TR/TE 7,819.57/110.27 ms, echo train length 63, flip angle 90°, FOV 70×70 mm, number of averages 5, slice thickness 5 mm, spacing between slices 5 mm, Bandwidth per pixel 1,330 Hz, matrix size 64×64, b-value 0, 1,400 s/mm^2.

Philips Ingenia 3T. T2-WI sequence. T2 TSE, TR/TE 4,438/110 ms, echo train length 17, flip angle 90°, FOV 300×300 mm, slice thickness 5 mm, number of excitations (NEX) 2, Bandwidth per pixel 218 Hz, matrix size 512×512. Diffusion-weighted imaging. Standard: TR/TE 4,000/80 ms, echo train length 31, flip angle 90°, FOV 300×300 mm, slice thickness 4 mm, Bandwidth per pixel 2,226 Hz, matrix size 176×176, b-value 0, 1,400 s/mm^2. MAR: TR/TE 4,000/80 ms, echo train length 31, flip angle 90°, FOV 220×220 mm, slice thickness 3 mm, Bandwidth per pixel 2,226 Hz, matrix size 176×176, b-value 0, 100, 700, 1,400, 2,000 s/mm^2. ZOOM: TR/TE 3,500/97 ms, echo train length 61, flip angle 90°, FOV 220×220 mm, slice thickness 3 mm, Bandwidth per pixel 2,204 Hz, matrix size 176×176, b-value 0, 100, 1,500 s/mm^2.

The approaches to reduce artifacts and setting the MAR scan protocol were the following: using SE sequences, increasing a number of averages (NEX, NAQ, ACQ), increasing a multiplicity of parallel data collection, choosing a smaller slice thickness, maximum extension of the receiver bandwidth. We chose the described above parameters according to the experience considering the physics of metal artifact and based on the literature sources (12,21,22). ZOOM program as the "ready-to-use" software protocol was used for Philips Ingenia 1.5T and 3T. This program has preconfigured small FOV imaging, SENSE parallel imaging technology ZOOM (9). The possibility of motion artifacts was addressed using tight fixation for the phantom.

We included a clinical case of a 72-year-old patient with right THR with MRI images acquired with a routine scanning protocol without special setting up. We also presented a clinical case of a 64-year-old patient after bilateral THR with MRI images acquired with an optimal scanning protocol to demonstrate a functioning of the adjusted protocols. The patients were recruited in Oncological Center No. 1 of Moscow City Hospital named after S.S. Yudin and Central Clinical Hospital "RZD-Medicine". The 72-year-old patient was referred for MRI by a urologist, PSA level =7 ng/mL. The study was performed on 1.5T Philips Ingenia scanner included T2 TSE WI sequence: TR/TE 3,750/90 ms, flip angle 90°,

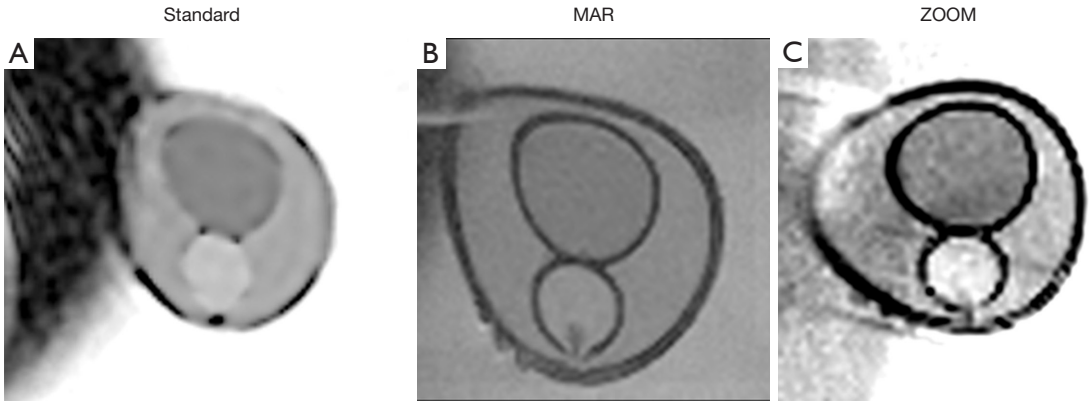

Figure 2 Philips 1.5T. (A) ADC Standard map, (B) ADC MAR map, (C) ADC ZOOM map. ADC, apparent diffusion coefficient; MAR, manual artifact reduction; ZOOM, title of software artifact reduction.

FOV 260×260 mm, slice thickness 4 mm, spacing between slices 5 mm, number of averages 1, Bandwidth per pixel 252 Hz, matrix size 350×350. Diffusion-weighted imaging: TR/TE 6,225/83 ms, echo train length 1, flip angle 90°, FOV 250×250 mm, number of averages 6, slice thickness 4 mm, spacing between slices 4, 8 mm, Bandwidth per pixel 1,300 Hz, matrix size 116×116, b-value 0, 1,200 s/mm^2. The 64-year-old patient was referred for MRI by a urologist, PSA level =7.5 ng/mL. The study was performed on 1.5T Philips Ingenia scanner included T2 TSE WI sequence: TR/TE 5,500/103 ms, flip angle 150°, FOV 260×260 mm, slice thickness 4 mm, spacing between slices 5 mm, number of averages 1, Bandwidth per pixel 140 Hz, matrix size 640×640. Diffusion-weighted imaging: TR/TE 4,100/104 ms, echo train length 1, flip angle 90°, FOV 250×250 mm, number of averages 6, slice thickness 4 mm, spacing between slices 4,8 mm, Bandwidth per pixel 2,210 Hz, matrix size 640×640, b-value 0, 1,200 s/mm^2.The following correction methods were applied: SE sequence, increased bandwidth, there are the following values: FOV reduction (260×260 mm), slice thickness reduction (4 mm). Overall scanning time for one patient was 30 minutes. A scanning protocol included T2-WI in the sagittal as well as coronal and axial planes. DWI were acquired in the axial plane followed by ADC maps calculation. The possibility of motion artifacts was addressed by properly preparing and positioning of the patient on the scan table.

The study was conducted in accordance with the Declaration of Helsinki (as revised in 2013), and was approved by the Independent Ethics Committee of the Moscow Regional Office of the Russian Society of Radiologists and Radiographists (approval number: 8, protocol code: 8/2022 and date of approval: 22.09.2022). Individual consent for this retrospective analysis was waived.

Analysis of results

All MRI images were reviewed by two radiologists with 13 and 5 years of experience in prostate MRI. The evaluation of the phantom functionality and experiment results were carried out qualitatively and quantitatively. First, a visual assessment of image quality changes as a result of using the adjusted protocol was performed. After visual assessment, the ADC values for both standard and adjusted imaging protocols (MAR, ZOOM) were quantified. A mean value and standard deviation (SD) of the signal in the corresponding sections were calculated. Mean values of ADC in the CZ, PZ and in the tumor ("Lesion") were measured on ADC maps (*Figure 1A*). The mean values and standard deviation for relative T2-WI signal and ADC were calculated based on the five repetitive evaluation made on the different slices. The indicators were compared with reference values.

Results

As a result of the experiment, after applying methods of artifact reduction, a decrease in the area and manifestation of scanning artifacts on ADC maps was observed (*Figures 2,3*).

The results of the quantitative assessment are presented in *Tables 1,2*.

Clinical applications

After setting up a protocol using the phantom, we had to

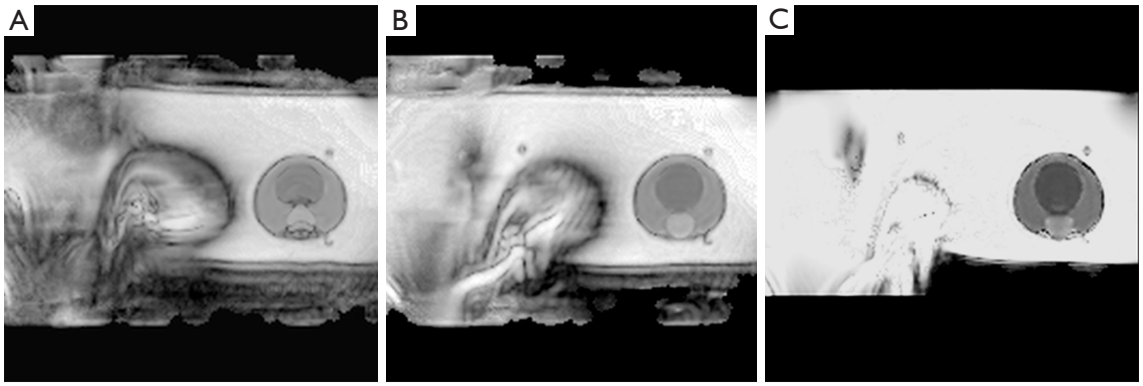

Figure 3 Philips 3T. (A) ADC standard map, (B) ADC MAR map, (C) ADC ZOOM map. ADC, apparent diffusion coefficient; MAR, manual artifact reduction; ZOOM, title of software artifact reduction.

Table 1 ADC values—Philips 1.5T

Parameter	CZ	PZ	"Lesion"
Standard, $\times 10^{-6}$ mm^2/s (mean ± SD)	1,062±7	1,334±4	1,519±7
MAR, $\times 10^{-6}$ mm^2/s (mean ± SD)	1,039±8	1,269±2	1,362±9
ZOOM, $\times 10^{-6}$ mm^2/s (mean ± SD)	1,030±14	1,146±38	1,365±16
ADC_{ref}, $\times 10^{-6}$ mm^2/s (mean ± SD)	1,000±36	1,230±39	1,410±36
Δ_{max}, %*	6.2	8.5	7.7

*, Δ_{max} = max [standard; MAR; ZOOM] × 100%/ADC_{ref}. ADC, apparent diffusion coefficient; CZ, central zone; PZ, peripheral zone; SD, standard deviation; MAR, manual artifact reduction; ZOOM, title of software artifact reduction; ADC_{ref}, the reference value of apparent diffusion coefficient.

Table 2 ADC values—Philips 3T

Parameter	CZ	PZ	"Lesion"
Standard, $\times 10^{-6}$ mm^2/s (mean ± SD)	1,279±3	1,546±3	1,774±58
Zoom, $\times 10^{-6}$ mm^2/s (mean ± SD)	1,304±3	1,573±4	1,821±40
MAR, $\times 10^{-6}$ mm^2/s (mean ± SD)	1,279±3	1,546±3	1,774±58
ADC_{ref}, $\times 10^{-6}$ mm^2/s	1,000	1,250	1,500
Δ_{max}, %*	30.4	25.8	21.4

*, Δ_{max} = max [standard; MAR; ZOOM] × 100%/ADC_{ref}. ADC, apparent diffusion coefficient; CZ, central zone; PZ, peripheral zone; SD, standard deviation; MAR, manual artifact reduction; ZOOM, title of software artifact reduction; ADC_{ref}, the reference value of apparent diffusion coefficient.

evaluate its effectiveness in scanning a patient. Without special setting up a scanning protocol, the images themselves are not diagnostically significant (*Figure 4*).

To demonstrate a functioning of the adjusted protocols, we present a clinical case of the patient after bilateral THR (*Figure 5*).

Discussion

ADC means and SDs were obtained across techniques for 1.5T and 3T. For 1.5T, the reduction in the influence of artifacts inside region of interest (ROI) was observed, expressed as a decrease in the average ADC (CZ, PZ,

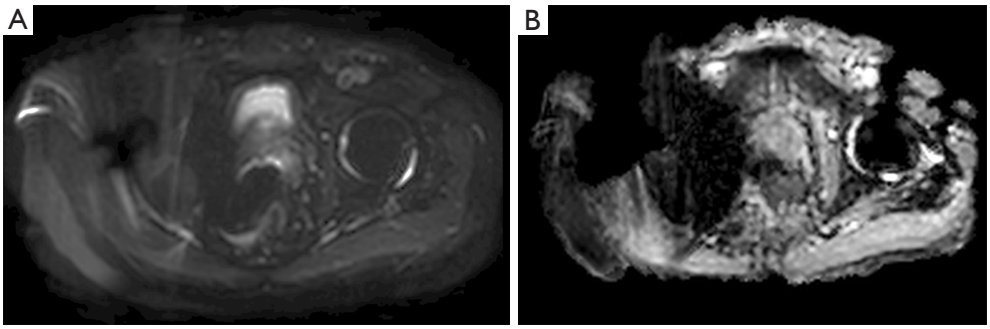

Figure 4 Prostate MRI. Male, 72 y.o., with total hip arthroplasty on the right: (A) DWI; (B) ADC map. MRI, magnetic resonance imaging; y.o., years old; DWI, diffusion-weighted images; ADC, apparent diffusion coefficient.

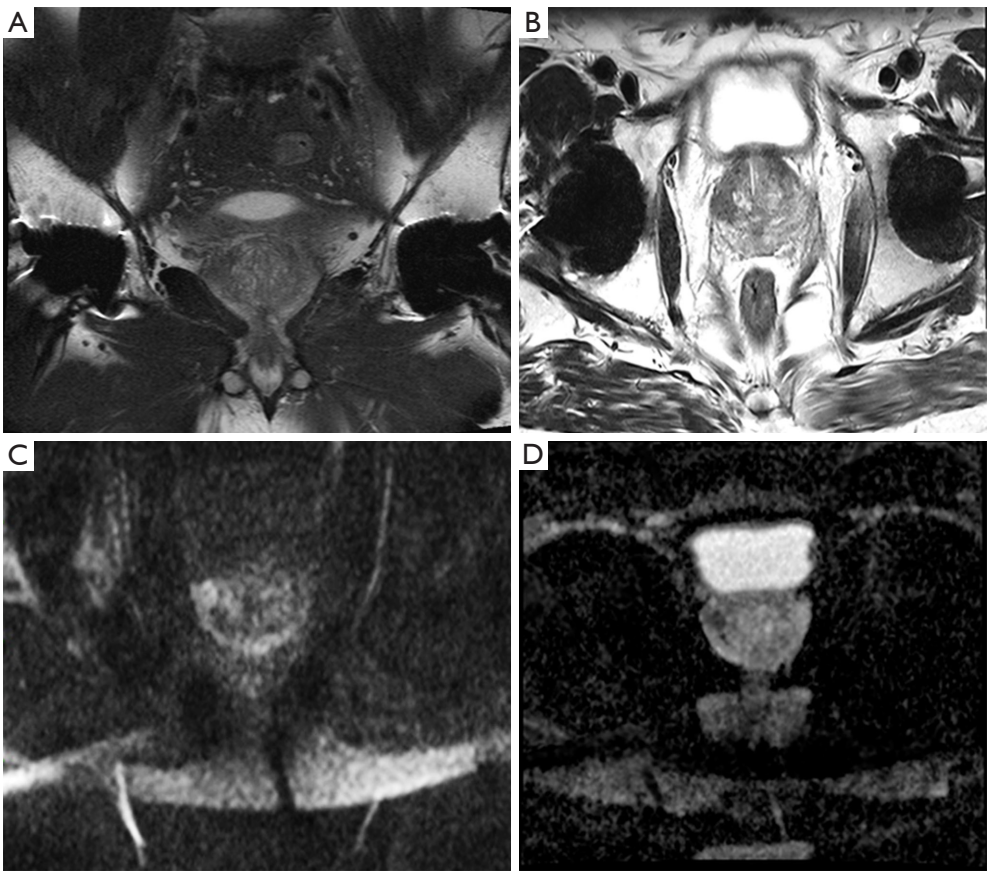

Figure 5 Prostate MRI. Male, 64 y.o., after bilateral total hip arthroplasty. (A) T2 FS WI coronal, (B) T2-WI axial, (C) DWI axial, b-value 1,200 s/mm^2, (D) ADC maps. In the base level of the right peripheral zone, the area of low signal is marked on T2-WI (A,B). In the base level of the right peripheral zone, there is the area of high signal on DWI (C) and low signal on ADC (D) with dimensions of 10×10 mm. MRI, magnetic resonance imaging; y.o., years old; FS, fat saturation; WI, weighted images; DWI, diffusion-weighted images; ADC, apparent diffusion coefficient.

"lesion") for the MAR and ZOOM techniques compared to the standard method. For example, Δmax, % for "lesion" was equal to 7.7% for Standard and –3.5% for MAR. For 3T this effect was not detected. The same ADC results were obtained for Standard and MAR techniques, and increased ADC values for ZOOM. This may be due to several factors: a larger FOV compared to that used for 1.5T and also a larger pixel value; a general increase in SNR when performing a 3 Tesla scan (this also explains the decrease in SD); a possible increase in ADC when scanning at 3T; as well as the ability to use several b-values for the 3T machines available to us. As can be seen from the table above, it is necessary to use a correction coefficient in the ADC calculation for the 3.0T device. We always recommend to apply a correction coefficient for deviations of more than 5% from the reference values. Thus, when setting the protocol, despite the fact that the spread of ADC values on 3.0T scanners was minimal, there was a significant deviation of ADC values from the reference ones (up to 30.4%). It confirms once again a relevance of applying the correction coefficient. In actual clinical practice, we decided not to increase the time of the patient's stay in the scanner. Increasing the scanning time could potentially lead to heating of the implants (23,24), as well as causing considerable discomfort to the patient. In the presented case, there are no illustrations showing artifacts from two hip endoprosthesis.

The algorithm for setting up a specialized prostate-examination protocol described in this study can be applied to any MRI study. Using SE sequences, increasing a number of averages (NEX, NAQ, ACQ), increasing a multiplicity of parallel data collection, choosing a smaller slice thickness, maximum extension of the receiver bandwidth and "ready-to-use" software protocol—are all universal tools for reducing artifacts from metal. It was clearly demonstrated by a clinical case of the patient who had MRI scanning after bilateral THR. This approach allows to reduce artifacts from hip implants, to visualize PG and periprostatic tissue in the best way, and to detect malignant and benign changes (11).

Prostate cancer is one of the leading causes of morbidity and mortality among men worldwide. This disease is more common in older men than in young men (25). In the United States, prostate cancer is the second leading cause of cancer mortality (26), in the European Union, it ranks the third one (27). Multiparameter magnetic resonance imaging (mpMRI) of the PG is a reliable tool for detecting clinically significant prostate cancer (CPG), thanks to which mpMRI has taken an important place in clinical practice (2). In particular, DWI correlate with a grade of the tumor malignancy according to the Gleason score. DWI is an indispensable sequence for assessing PG, especially the peripheral zone, where 75–80% of clinically significant prostate cancer is located (11,28,29).

Metal hip implants are proven source of significant artifacts in DWI. DWI, being the basis for the assessment of PI-RADS, play the important role in making a diagnosis and choosing a tactics of patient treatment (whether it can be active observation, surgery, radiation therapy, etc.) (2,20,30). DWI is the most sensitive sequence to metallic artifacts (5). Artifacts' presence makes a study uninformative, preventing adequate visualization of the PG and potentially making follow-up observation impossible (*Figure 4*). Thus, the development of methods to improve a quality of DWI of prostate in patients with implants is of great clinical importance (1,13,17). Arthroplasty is a generally accepted standard method of treatment for end-stage hip arthritis. The age group of patients with end-stage arthritis coincides with the group of patients with prostate cancer. It is expected that by 2030 a number of arthroplasty procedures for large joints will double, making this problem even more serious (31).

Rosenkrantz *et al.* notes the possibility of improving the image quality on 3.0T scanners when using DWI with reduced view field (rFOV) with parallel visualization (32). For example, in the study of Czarniecki *et al.*, the PROPELLER program based on alternative methods for filling k-space (non-Cartesian filling of k-space) was demonstrated (11). Most manufacturers have their own trade names for pulse sequences based on this method—PROPELLER (GE), BLADE (Siemens), MulitVane (Philips), RADAR (Hitachi) и JET (Canon). If these solutions are available, they should be included in the scanning protocol for patients with artificial metal implants. Despite the possibility of performing a study on scanners with a magnetic field induction of 3.0T, patients after THR surgery are recommended to perform a study on 1.5T scanners, since in this case the study will not have such strong distortions.

Despite the fact that approaches to minimizing artifacts are universal for any scanner, each scanner is required to be set up particularly. To conduct a highly informative study, radiologists should be familiar with all the nuances of study planning (5,33). In the case of patients with hip implants, it is required to generate new individual scanning protocols. However, this process will take a significant amount of time. It will cause a patient to stay in the scanner for a long time,

and a department operation will be disrupted. Besides that, as the scan duration increases, the risk of excessive implant heating increases (16). The phantom, we have developed, can allow fine-tuning a scanning protocol in advance and for various situations (for different types of implants, different numbers, for example, for single-or bilateral hip replacement, etc.).

Our study has also certain limitations. In this study, since the phantom lacked anthropomorphic features, it was not meant to fully simulate the human pelvis. Because of this, it was impossible to assess how surrounding fatty tissue affects the quantitative measures. Modeling of the difference in relaxation times of prostate tissues was not performed (only the difference in the diffusion coefficient), therefore, on T1-WI, T2-WI, DWI, the "gland" zones (CZ, PZ, "Lesion") are indistinguishable from each other. A simulation of different relaxation times is beyond the scope of this study. If necessary, this issue can be resolved by adding some amount of calcium or magnesium salts to PVP solutions. Probably, to some extent, different results could be obtained using the anthropomorphic phantom as a corpus. This issue will be investigated in the continuation of this study. There are no data on visualization of the phantom on scanners from other manufacturers due to the limited information on available scanners. The mean ADC values were calculated by the b-value. In this case, the voxel size, which was different in the scan, contributes to the noise indicator. We also added this to the discussion of the results (from *Tables 1*,*2* it can be seen that for 3T the noise is less, which may be due to both the higher magnetic field induction and the larger voxel size). Manufacturers apply different combinations of correction methods, thereby complicating the unification of approaches and recommendations. However, it is beyond the scope of this study. The absence of cross-calibration makes multicenter studies impossible. Of course, in order to implement it into practice, the application of correction coefficients should be automated (especially since there might be several of them for different ranges of ADC values). However, this issue is beyond the scope of this study. Cause of different applied sequences [such as manually edited (MAR) and automatic option (ZOOM)], the scan parameters were not accurately equal. However, this limitation does not influence the achieved purpose of this study.

In this paper, we designed a system to model quantitative parameters, developed a physical model, and demonstrated the possibility to acquire images in presence of metal implants without sacrificing the quality. Such an integrated approach opened the way to perform MRI studies in patients with metal implants. If in the future, with the improvement of prostate diagnostics and replacement of the qualitative assessment with the quantitative one, using this phantom, a correction coefficient can be calculated (19,34). Using ADC with a sufficient degree of accuracy and reliability requires technical progress and systematic quality control. Standardization of measurements is critical to overcome the issue of ADC variability (35). One of the means of quality control is phantom modeling, which is the optimal for such numerical quantitative ADC (19). In the future, the study requires further validation, patients with biopsy-confirmed diagnosis.

Conclusions

Thorough attention to planning a prostate scanning protocol is essential for the detection, localization, diagnosis of prostate cancer and stratification of its risk in patients with metal implants. The developed phantom can allow to generate scanning protocols in advance while controlling the qualitative and quantitative scanning parameters. Using phantoms for presetting a protocol ensures diagnostic quality and patient comfort.

Acknowledgments

This paper was prepared by a group of authors as a part of the research and development effort titled "Research program to further the standardization, safety and quality of magnetic resonance imaging" (USIS No. 123031500007-6) in accordance with the Order No. 1196 dated December 21, 2022 "On approval of state assignments funded by means of allocations from the budget of the city of Moscow to the state budgetary (autonomous) institutions subordinate to the Moscow Health Care Department, for 2023 and the planned period of 2024 and 2025" issued by the Moscow Health Care Department.
Funding: None.

Footnote

Conflicts of Interest: All authors have completed the ICMJE uniform disclosure form (available at https://qims.amegroups.com/article/view/10.21037/qims-24-604/coif). All authors report that this paper was prepared by a group of authors as a part of the research and development effort titled "Research program to further the standardization,

safety and quality of magnetic resonance imaging" (USIS No. 123031500007-6) in accordance with the Order No. 1196 dated December 21, 2022 "On approval of state assignments funded by means of allocations from the budget of the city of Moscow to the state budgetary (autonomous) institutions subordinate to the Moscow Health Care Department, for 2023 and the planned period of 2024 and 2025" issued by the Moscow Health Care Department. K.A.S. is affiliated with CAPSTROYCITY. The authors have no other conflicts of interest to declare.

Ethical Statement: The authors are accountable for all aspects of the work in ensuring that questions related to the accuracy or integrity of any part of the work are appropriately investigated and resolved. The study was conducted in accordance with the Declaration of Helsinki (as revised in 2013), and was approved by the Independent Ethics Committee of the Moscow Regional Office of the Russian Society of Radiologists and Radiographists (approval number: 8, protocol code: 8/2022 and date of approval: 22.09.2022). Individual consent for this retrospective analysis was waived.

References

1. Engels RRM, Israël B, Padhani AR, Barentsz JO. Multiparametric Magnetic Resonance Imaging for the Detection of Clinically Significant Prostate Cancer: What Urologists Need to Know. Part 1: Acquisition. Eur Urol 2020;77:457-68.
2. Padhani AR, Weinreb J, Rosenkrantz AB, Villeirs G, Turkbey B, Barentsz J. Prostate Imaging-Reporting and Data System Steering Committee: PI-RADS v2 Status Update and Future Directions. Eur Urol 2019;75:385-96.
3. Gawlitza J, Reiss-Zimmermann M, Thörmer G, Schaudinn A, Linder N, Garnov N, Horn LC, Minh DH, Ganzer R, Stolzenburg JU, Kahn T, Moche M, Busse H. Impact of the use of an endorectal coil for 3 T prostate MRI on image quality and cancer detection rate. Sci Rep 2017;7:40640.
4. Gelezhe PB, Blokhin IA, Semenov SS, Caruso D. Magnetic resonance imaging radiomics in prostate cancer radiology: what is currently known? Digital Diagnostics 2021;2:441-52.
5. Caglic I, Barrett T. Optimising prostate mpMRI: prepare for success. Clin Radiol 2019;74:831-40.
6. Jambor I. Optimization of prostate MRI acquisition and post-processing protocol: a pictorial review with access to acquisition protocols. Acta Radiol Open 2017;6:2058460117745574.
7. Artifacts from metal structures in magnetic resonance imaging. Best Pract. Moscow: Research and Practical Clinical Center for Diagnostics and Telemedicine Technologies of the Moscow Healthcare Department, 2022.
8. Matharu GS, Kunutsor SK, Judge A, Blom AW, Whitehouse MR. Clinical Effectiveness and Safety of Aspirin for Venous Thromboembolism Prophylaxis After Total Hip and Knee Replacement: A Systematic Review and Meta-analysis of Randomized Clinical Trials. JAMA Intern Med 2020;180:376-84.
9. Rosenkrantz AB, Chandarana H, Pfeuffer J, Triolo MJ, Shaikh MB, Mossa DJ, Geppert C. Zoomed echo-planar imaging using parallel transmission: impact on image quality of diffusion-weighted imaging of the prostate at 3T. Abdom Imaging 2015;40:120-6.
10. Brendle C, Martirosian P, Schwenzer NF, Kaufmann S, Kruck S, Kramer U, Notohamiprodjo M, Nikolaou K, Schraml C. Diffusion-weighted imaging in the assessment of prostate cancer: Comparison of zoomed imaging and conventional technique. Eur J Radiol 2016;85:893-900.
11. Czarniecki M, Caglic I, Grist JT, Gill AB, Lorenc K, Slough RA, Priest AN, Barrett T. Role of PROPELLER-DWI of the prostate in reducing distortion and artefact from total hip replacement metalwork. Eur J Radiol 2018;102:213-9.
12. Hargreaves BA, Worters PW, Pauly KB, Pauly JM, Koch KM, Gold GE. Metal-induced artifacts in MRI. AJR Am J Roentgenol 2011;197:547-55.
13. Zhang L, Zhe X, Tang M, Zhang J, Ren J, Zhang X, Li L. Predicting the Grade of Prostate Cancer Based on a Biparametric MRI Radiomics Signature. Contrast Media Mol Imaging 2021;2021:7830909.
14. Abreu-Gomez J, Walker D, Alotaibi T, McInnes MDF, Flood TA, Schieda N. Effect of observation size and apparent diffusion coefficient (ADC) value in PI-RADS v2.1 assessment category 4 and 5 observations

compared to adverse pathological outcomes. Eur Radiol 2020;30:4251-61.
15. Esen M, Onur MR, Akpolat N, Orhan I, Kocakoc E. Utility of ADC measurement on diffusion-weighted MRI in differentiation of prostate cancer, normal prostate and prostatitis. Quant Imaging Med Surg 2013;3:210-6.
16. Winter L, Seifert F, Zilberti L, Murbach M, Ittermann B. MRI-Related Heating of Implants and Devices: A Review. J Magn Reson Imaging 2021;53:1646-65.
17. Abuladze LR, Semenov DS, Panina OY, Vasilev YA. Optimized biparametric magnetic resonance imaging protocol for prostate cancer detection. Digit Diagnostics 2022;3:166-77.
18. Semenov DS, Petryaykin AV, Vasiliev YA, Akhmad ES, Panina OY. Phantom blueprint for setting up magnetic resonance imaging protocols of the prostate gland in patients with metal implants in the hip joint. Moscow; Patent Report No.: Utility model patent No. RU 208239 U1, the Russian Federation.
19. Morozov S, Sergunova K, Petraikin A, Akhmad E, Kivasev S, Semenov D, Blokhin I, Karpov I, Vladzymyrskyy A, Morozov A. Diffusion processes modeling in magnetic resonance imaging. Insights Imaging 2020;11:60.
20. Zhang Y, Holmes J, Rabanillo I, Guidon A, Wells S, Hernando D. Quantitative diffusion MRI using reduced field-of-view and multi-shot acquisition techniques: Validation in phantoms and prostate imaging. Magn Reson Imaging 2018;51:173-81.
21. Jungmann PM, Agten CA, Pfirrmann CW, Sutter R. Advances in MRI around metal. J Magn Reson Imaging 2017;46:972-91.
22. Khodarahmi I, Isaac A, Fishman EK, Dalili D, Fritz J. Metal About the Hip and Artifact Reduction Techniques: From Basic Concepts to Advanced Imaging. Semin Musculoskelet Radiol 2019;23:e68-81.
23. Methodology for assessing a heating of passive implants caused by exposure to a radio-frequency field during magnetic resonance imaging. Best Pract. Moscow: Research and Practical Clinical Center for Diagnostics and Telemedicine Technologies of the Moscow Healthcare Department, 2020.
24. Fundamentals of safety during magnetic resonance imaging. Best Pract. Moscow: Research and Practical Clinical Center for Diagnostics and Telemedicine Technologies of the Moscow Healthcare Department, 2019.
25. Tammisetti VS. MR safety considerations for patients undergoing prostate MRI. Abdom Radiol (NY) 2020;45:4097-108.
26. Siegel RL, Miller KD, Fuchs HE, Jemal A. Cancer Statistics, 2021. CA Cancer J Clin 2021;71:7-33.
27. Ferlay J, Colombet M, Soerjomataram I, Dyba T, Randi G, Bettio M, Gavin A, Visser O, Bray F. Cancer incidence and mortality patterns in Europe: Estimates for 40 countries and 25 major cancers in 2018. Eur J Cancer 2018;103:356-87.
28. Merisaari H, Toivonen J, Pesola M, Taimen P, Boström PJ, Pahikkala T, Aronen HJ, Jambor I. Diffusion-weighted imaging of prostate cancer: effect of b-value distribution on repeatability and cancer characterization. Magn Reson Imaging 2015;33:1212-8.
29. Tang L, Zhou XJ. Diffusion MRI of cancer: From low to high b-values. J Magn Reson Imaging 2019;49:23-40.
30. Lo GC, Margolis DJA. Prostate MRI with PI-RADS v2.1: initial detection and active surveillance. Abdom Radiol (NY) 2020;45:2133-42.
31. Kurtz S, Ong K, Lau E, Mowat F, Halpern M. Projections of primary and revision hip and knee arthroplasty in the United States from 2005 to 2030. J Bone Joint Surg Am 2007;89:780-5.
32. Rosenkrantz AB, Taneja SS. Use of Reduced Field-of-View Acquisition to Improve Prostate Cancer Visualization on Diffusion-Weighted Magnetic Resonance Imaging in the Presence of Hip Implants: Report of 2 Cases. Curr Probl Diagn Radiol 2018;47:125-7.
33. Mussi TC, Baroni RH, Zagoria RJ, Westphalen AC. Prostate magnetic resonance imaging technique. Abdom Radiol (NY) 2020;45:2109-19.
34. Brunese L, Mercaldo F, Reginelli A, Santone A. Formal methods for prostate cancer Gleason score and treatment prediction using radiomic biomarkers. Magn Reson Imaging 2020;66:165-75.
35. Moreau B, Iannessi A, Hoog C, Beaumont H. How reliable are ADC measurements? A phantom and clinical study of cervical lymph nodes. Eur Radiol 2018;28:3362-71.

Cite this article as: Vasilev YA, Panina OY, Semenov DS, Akhmad ES, Sergunova KA, Kivasev SA, Petraikin AV. Prostate magnetic resonance imaging (MRI) in patients with hip implants—presetting a protocol using a phantom. Quant Imaging Med Surg 2024;14(10):7128-7137. doi: 10.21037/qims-24-604

